Detection of Prenatal Alcohol Exposure Using Machine Learning Classification of Resting-State Functional Network Connectivity Data

Carlos I. Rodriguez, Ph.D.[1], Victor Vergara, Ph.D.[2], Suzy Davies, Ph.D.[3], Vince Calhoun, Ph.D.[2,1] Daniel D. Savage, Ph.D.[3,4], Derek A. Hamilton, Ph.D.[3,4]

Affiliations

1. The Mind Research Network. 1101 Yale Blvd. NE, Albuquerque, NM, 87106, USA.
2. Tri-Institutional Center for Translational Research in Neuroimaging and Data Science (TReNDS), Georgia State University, Georgia Institute of Technology, and Emory University. 55 Park Pl NE, Atlanta, GA 30303, USA.
3. Department of Neurosciences, University of New Mexico School of Medicine. 1 University of New Mexico, Albuquerque, NM, 87131, USA.
4. Department of Psychology, University of New Mexico. 1 University of New Mexico, Albuquerque, NM 87131, USA.

Running Title: Classification of Prenatal Alcohol Exposure

***Corresponding Author**:*

Carlos I. Rodriguez

The Mind Research Network

1101 Yale Boulevard Northeast

Albuquerque, NM 87106

Phone: 505-301-5483

Email: crodriguez@mrn.org

Keywords: Prenatal Alcohol Exposure, Fetal Alcohol Spectrum Disorder, Machine Learning, Functional Network Connectivity

ABSTRACT

Fetal Alcohol Spectrum Disorder (FASD), a wide range of physical and neurobehavioral abnormalities associated with prenatal alcohol exposure (PAE), is recognized as a significant public health concern. Advancements in the diagnosis of FASD have been hindered by a lack of consensus in diagnostic criteria and limited use of objective biomarkers. Previous research from our group utilized resting state functional magnetic resonance imaging (fMRI) to measure functional network connectivity (FNC) revealed several sex- and region-dependent alterations in FNC as a result of moderate PAE relative to controls. Considering that FNC is sensitive to moderate PAE, this study explored the use of FNC data and machine learning methods to detect PAE among a sample of rodents exposed to alcohol prenatally and controls. We utilized previously acquired resting state fMRI data collected from adult rats exposed to moderate levels of prenatal alcohol (PAE) or a saccharin control solution (SAC) to assess FNC of resting state networks extracted by spatial group independent component analysis (GICA). FNC data was subjected to binary classification using support vector machine (SVM)-based algorithms and leave-one-out-cross validation (LOOCV) in an aggregated sample of males and females (n=48; 12 male PAE, 12 female PAE, 12 male SAC, 12 female SAC), a males only sample (n=24; 12 PAE, 12 SAC), and a females only sample (n=24; 12 PAE, 12 SAC). Results revealed that a quadratic SVM (QSVM) kernel was significantly effective for PAE detection in females. QSVM-kernel-based classification resulted in accuracy rates of 62.5% for all animals, 58.3% for males, and 79.2% for females. Additionally, qualitative evaluation of QSVM weights implicate an overarching theme of several hippocampal and cortical networks in

contributing to the formation of correct classification decisions by QSVM. Our results suggest that binary classification using QSVM and adult female FNC data is a potential candidate for the translational development of novel and non-invasive techniques for the identification of FASD.

ACRONYMS

BOLD	Blood Oxygen Level Dependent
FAS	Fetal Alcohol Syndrome
FASD	Fetal Alcohol Spectrum Disorder
fMRI	function Magnetic Resonance Imaging
FNC	Functional Network Connectivity
FWHM	Full Width Half Max
GICA	Group Independent Components Analysis
GIFT	Group ICA of fMRI Toolbox
HPA	Hypothalamic Pituitary Adrenal Axis
LOOCV	Leave One Out Cross Validation
MLP	Multilayer Perceptron
NMDA	N-methyl-D-Aspartate

PAE	Prenatal Alcohol Exposure
QSVM	Quadratic SVM
RBF	Radial Basis Function
RSN	Resting State Network
SAC	Saccharin
SVM	Support Vector Machine

INTRODUCTION

Fetal alcohol spectrum disorder (FASD) is a term that is utilized to encompass a wide range of morphological and neuro-behavioral phenotypes caused by prenatal alcohol exposure [PAE, (Loock et al., 2005; Williams, Smith, & Committee On Substance, 2015)]. The most severe phenotype is known as Fetal Alcohol Syndrome (FAS) and is linked to heavy prenatal alcohol exposure (PAE) (Lemoine, Harousseau, Borteyru, & Menuet, 1968; Manning & Eugene Hoyme, 2007). Children with FAS exhibit facial dysmorphologies, growth deficits, and numerous impairments in cognitive and behavioral functions related to attention, learning, memory, and motor coordination among others (Connor et al., 2000; Jones & Smith, 1973, 1975; Streissguth et al., 1986). Although the most severe, FAS is the least common FASD with an estimated prevalence rate of ~0.1% in the U.S. (May & Gossage, 2001). However, when considering the entire spectrum, estimated prevalence rates of FASD (including FAS) fall between 1.1% and 5.0% of U.S. children, many of which will not display readily identifiable facial dysmorphologies, but may nonetheless exhibit cognitive and behavioral impairments (May et al., 2014; May et al., 2018). Unfortunately, children who do not display the cardinal facial features characteristic of FAS, may fail to receive a timely diagnosis which can prevent securing the appropriate treatment or support services (Bertrand et al., 2005) and increase the likelihood of experiencing negative life outcomes related to academic success (Mattson & Riley, 1998), difficulty in finding and maintaining meaningful employment, and staying out of trouble with the law (Popova et al., 2011). In addition, disagreement among diagnostic criteria and a lack of clinical expertise contribute to challenges in identifying individuals with FASD (Mattson, Bernes,

& Doyle, 2019). As a result, novel diagnostic approaches for FASD may possess clinical utility that may lead to improved outcomes.

From the early clinical descriptions of FAS (Jones & Smith, 1973, 1975), research with human participants has been critical for understanding the social, physical, and neuro-behavioral sequelae of PAE (Connor et al., 2000; Streissguth et al., 2004). However, variables such as dose (e.g., high, moderate, low), timing (e.g., 1st, 2nd trimester), and pattern of alcohol exposure (e.g., daily vs binge), can be difficult to account for and, for ethical reasons, are impossible to experimentally manipulate in human subjects research (Patten, Fontaine, & Christie, 2014). To overcome these challenges, animal models of FASD have been important for illuminating the underlying neurobiological consequences associated with developmental alcohol exposure.

Considering that children are more likely to be exposed to moderate, rather than heavy, levels of prenatal alcohol exposure (May et al., 2018; May & Gossage, 2001), animal research aimed at studying the effects of moderate PAE is extremely valuable because it closely mimics the pattern of alcohol exposure observed in the human population. Within animal models of PAE, considerable work has been undertaken with the aim of investigating discrete brain areas such as the hippocampus (Gil-Mohapel, Boehme, Kainer, & Christie, 2010; Savage, Becher, de la Torre, & Sutherland, 2002) and cerebellum (Servais et al., 2007). However, higher level cognitive and behavioral functions, including those associated with FASD, involve sophisticated and highly coordinated activity across multiple, rather than single, brain regions (Green et al., 2009). Functional network connectivity (FNC) methods (i.e. functional connectivity between coherent brain networks) offer an important lens that can be leveraged to

understand the temporal statistical dependencies (e.g. correlations) of multiple and distant brain networks (Arbabshirani & Calhoun, 2011) following PAE. Functional magnetic resonance imaging (fMRI), a neuroimaging modality employed to non-invasively measure blood-oxygenation-level dependent (BOLD) signals that reflect patterns of neuronal activity (Logothetis et al., 2001; Raichle & Mintun, 2006), has been widely utilized to derive measures of FNC (Allen et al., 2011). Group level fMRI data gathered at rest, an experimental condition that lacks externally presented stimuli or behavioral responses (Snyder & Raichle, 2012), can be examined by group independent component analysis (GICA). As a blind source separation algorithm, GICA is a data driven technique that extracts the temporal activation patterns (time courses) of resting state networks (RSNs) where each network may consist of multiple brain regions (Allen et al., 2011; Arbabshirani & Calhoun, 2011; Buckner, Krienen, & Yeo, 2013). The FNC assessment consists of correlations between the time-courses of brain networks. Brain dysfunction can then be identified by abnormal correlations (e.g. too high or too low) when comparing FNC across control and experimental treatment conditions. Our group previously applied GICA to resting state fMRI data acquired from adult rodents exposed to moderate levels of PAE that revealed several sex and regionally dependent alterations in FNC (Rodriguez et al., 2016a) which point to FNC is a potential biomarker that can be used concurrently with machine learning for the identification of PAE.

Machine learning is a topic of growing interest to the scientific community. It encompasses a wide range of statistical and computational techniques that can model the complex and nonlinear relationships between predictor variables. Machine learning

is well suited for “wide” data sets in which the number of predictor variables exceeds the number of subjects (Bzdok, Altman, & Krzywinski, 2018) and generally emphasizes prediction rather than explanation, even at the expense of interpretability (Breiman, 2001; Yarkoni & Westfall, 2017). Machine learning methods can be broadly categorized into two classes, supervised and unsupervised learning (Bastanlar & Ozuysal, 2014; Hastie, 2009). In unsupervised learning, the aim is to develop a model that can describe associations and patterns among a set of predictor variables (Hastie, 2009). In supervised learning, both outcome and predictors variables are used to develop models that can later be used on novel data, of the same structure, to predict an outcome. The process of building a model algorithmically is referred to as training, while deploying the developed model on data not included in the training phase is referred to as testing. Features represent the predictor variables of the input data used in training, while outcomes represent the predicted output variables (Bastanlar & Ozuysal, 2014). Outcome variables can take on quantitative or qualitative values. When output variables take on a set of discrete labels, the predictive model is called a classifier. A binary classifier specifically refers to a model that predicts a variable adopting only one of two discrete outcome values often referred to as labels. Classifiers can then be evaluated based on how well they predict an outcome variable when deployed on test data (Choi et al., 2020).

The discovery of phenotypic, biological, and psychometric markers related to PAE has motivated explorations of machine learning methods for detecting FASD in clinical settings. Fang and colleagues used facial dysmorphology data and binary classification to identify facial features that discriminate between FAS and control

participants (Fang et al., 2008). Zhang and colleagues used psychometric, eye tracking, and structural MRI data alone and in combination to detect FASD (Zhang et al., 2019). Utilizing the same psychometric data set as Zhang et al., 2019, artificial neural networks proved useful in identifying individuals with FASD (Duarte, 2020). Machine learning has also been utilized to detect FASD in children and adolescents solely from structural MRI data (Little & Beaulieu, 2020). However, the utility of machine learning for the detection of FASD from fMRI connectivity data remains to be determined.

In this study, we explore the use of binary-classification algorithms to detect PAE among a mixed sample of FNC data from rodents with PAE and controls. The effectiveness of the implemented binary-classifiers was tested using leave-one-out-cross validation (LOOCV). Functional neuroimaging data were obtained from our previously published report that characterized the effects of moderate PAE on FNC by utilizing GICA of resting-state fMRI data (Rodriguez et al., 2016a). The primary goal of this current investigation was to explore the utility of machine learning algorithms as a novel and non-invasive means to classify aberrant brain connectivity patterns associated with PAE.

METHODS

Subjects

Subjects, materials, and procedures were previously reported in separate studies approved by the Institutional Animal Care and Use Committee of the University of New Mexico main campus and Health Sciences Center (Rodriguez et al., 2016a; Rodriguez et al., 2016b). Briefly, 48 Long-Evans rats (24 SAC and 24 PAE; 24 males and 24 females) were generated in a single breeding round designed to prenatally expose rats

to either a 5% ethanol (v/v) or 0.066% saccharin solution (Hamilton et al., 2014) for the duration of the entire 21-day gestational period. Following weaning, animals were housed with an age- and weight-matched cagemate from the same prenatal treatment, but different litter, in standard plastic cages with water and food available ad libitum.

At 3-4 months of age, all animals underwent a series of structural- and blood oxygenation level dependent (BOLD) fMRI-scan sequences under isoflurane anesthesia for ~45 min in a 4.7T Bruker Biospin (Billerica, MA) MRI scanner. Functional MRI data were acquired with a 10-minute echo planar imaging acquisition at a temporal resolution (TR) of 2 sec (FOV = 3.84 cm x 3.84 cm, matrix = 64 x 64, TE = 21.3 ms, flip angle = 90°, 27 slices, and slice thickness = 1 mm).

Image Preprocessing, Group Independent Component Analysis (GICA), and Functional Network Connectivity

Preprocessing, GICA, and FNC methods are described in (Rodriguez et al., 2016a). To summarize, fMRI data preprocessing included realignment, spatial normalization to the Paxinos & Watson atlas (Schweinhardt et al., 2003), and smoothing with a 0.5 mm full-width-half-maximum (FWHM) Gaussian kernel in Statistical Parametric Mapping 8 (SPM8) (Wellcome Department of Cognitive Neurology, London, UK) running in MATLAB (Mathworks, Inc., Natick, MA) version R2012b. After preprocessing, 40 group-level independent components were extracted utilizing the Infomax algorithm (Bell & Sejnowski, 1995) in the Group ICA of fMRI Toolbox (GIFT, www.trendscenter.org/software/gift) (Calhoun, Adali, Pearlson, & Pekar, 2001). Of the initial 40 components, 17 components were retained based on the exclusion of

components localized to white matter tracts or cerebro-spinal fluid and the presence of artifactual features upon visual inspection.

In this study, component time courses were orthogonalized with respect to the following: (1) linear, quadratic, and cubic trends; (2) the six realignment parameters (translation in the x, y, and z directions and rotations about the x, y, z axes); and the 6 realignment parameter derivatives. Time-courses were lowpass filtered with a cutoff at 0.15Hz. Functional network connectivity (FNC) measures were estimated from pairwise correlations between average individual component time-courses for each rat. A total of 136 unique pairwise correlations were calculated for each animal given by the following: $(\frac{C*(C-1)}{2})$ where *C* = 17 (the number of retained components). Thus, the structure of the FNC data utilized for machine learning procedures consisted of 48 correlation matrices, one from each rodent. All correlation values were Fisher's Z transformed for subsequent analyses and served as features during machine learning training. Retained components are displayed in Figure 1 and the anatomical location for the peak value of each component, in Paxinos and Watson space, is displayed in Table 1 (Paxinos & Watson, 2004). However, these components and their location were previously reported in an earlier study and do not represent results from an independent investigation (Rodriguez et al., 2016a). Components are displayed to aid in localizing the brain regions from which the FNC measures for this study were derived from.

Machine Learning Procedures

The machine learning methods to classify FNC patterns between PAE and SAC animals were based on work previously described in (Vergara, Mayer, Kiehl, & Calhoun, 2018) and relied on utilizing FNC data from GICA-extracted components. As reported in Vergara and colleagues (2018) SVM tuning parameters were set to a least squares solving method, a soft margin parameter of 0.1 and a feature selection threshold of absolute value of 0.75. Feature selection was implemented by conducting a two-sample t-test on SAC and PAE groups for each of the 136 FNC values and discarding FNCs with a t-value failing to meet the $|t| = 0.75$ threshold. The use of t-tests was not implemented to statistically compare groups as those analyses were reported in a previous investigation (Rodriguez et al., 2016a). Instead, the resulting t-values were used to select a subset of FNC features with the aim of guarding against overfitting and improving generalizability of the computational models. This SVM configuration was used to test five different SVM kernels: linear, quadratic (QSVM), cubic, radial basis functions (RBF) and multilayer perceptron (MLP) kernels in MATLAB (Mathworks, Inc., Natick, MA) version 2016b to perform binary classification of FNC data at the subject level. Because of the relatively small sample size, leave-one-out cross validation (LOOCV) was chosen to assess classification performance. The LOOCV procedure consisted of isolating one sample for testing and the remainder of the samples for training across multiple iterations as displayed in Figure 2. Statistical significance of accuracy rates was assessed by a permutation test approach in which the prenatal condition labels of individual subject's FNC data were randomized and subsequently subjected to 10,000 replications of QSVM classification and LOOCV with random

groups on each replication to establish the null probability distribution of accuracy rates from randomized data (null model). Significance at the p = 0.01 level (Bonferroni corrected α=.05/5, accounting for the five kernels tested) was estimated from the null distribution. Finally, to address classification performance within each sex separately, the permutation test approach and LOOCV procedures were repeated for subsets of male and female only data.

RESULTS

Table 2 displays the accuracy rates of multiple kernels used in SVM binary classification. The quadratic kernel demonstrated the highest classification rates when classifying all (both male and female samples; 62.5%) and female samples only (79.2%). The quadratic and RBF kernels demonstrated the highest accuracy rates for male samples (58.3 %). The lowest accuracy rates were observed for all samples using the RBF kernel (50%), males using the linear kernel (50%) and for females a three-way tie (66.7%) among linear, cubic, and MLP kernels. The quadratic SVM (QSVM) kernel displayed the best overall accuracy rates for discriminating between alcohol- and saccharin exposed animals and was therefore chosen for the remaining series of analyses.

Figure 3 displays accuracy-rate histograms after the prenatal conditions of FNC data were randomized and subjected to 10,000 iterations of QSVM classification and LOOCV to establish null distributions. Each null distribution was used to estimate the adjusted p=0.01 level threshold of statistical significance for accuracy rates of QSVM classification in all (A), female (B), and male samples (C). The significance threshold for all samples was 63%. The accuracy rate for all animals in QSVM classification (62.5%)

was not significant. For females, the significance threshold was estimated at 75% thus the QSVM classification rate for females (79.2%) was statistically significant. Finally, the significance threshold for males was 71%, rendering the QSVM's performance for classifying males (58.3%) as not statistically significant. To verify that the permutation tests were not influenced by FNC couplings with unequal variances, we performed a supplementary analysis consisting of a series of Levene's tests for equality of variance on the female data. The results of these tests are displayed in Supplementary Figure 1 and revealed no significant differences of variance between PAE and SAC females. This analysis was important to verify that the permutation results were not influenced by differences in group variability.

Figure 4 displays a series of matrices that display the percentage of times that each FNC value met the feature selection threshold during all iterations of LOOCV for all animals (A), females (B), and males (C). For all animals, a total of 48 iterations of LOOCV were conducted, whereas LOOCV was conducted over 24 iterations separately for male and female animals. These matrices indicate which FNC couplings were typically used as features for training with the five separate SVM kernels.

The QSVM assigns weights to each FNC feature in each iteration used in classification. Mean classification weights are displayed in Figure 5 for all samples(A), females (B), and males (C). Weights can be used to explore the contributions of specific component correlations that most strongly impact correct classification decisions. For all samples, a general pattern of moderately positive weights results from network correlations between cerebellar-hippocampal connectivity. Other moderate positive weights result from couplings in hippocampal-striatal, hippocampal-cortical, and

hippocampal-midbrain components, while a strong mean positive weight was found in a hippocampal-thalamic coupling consisting of components with peak activations localized to the ventral-anterior thalamus and the dentate gyrus of the hippocampus. Strong negative weights result from cerebellar-cortical, hippocampal-midbrain, and cortical-striatal couplings. For males, strong and moderately strong positive weights cluster in cortical-midbrain, cortical-hippocampal, cortical-cortical, cerebellar-hippocampal, and hippocampal-thalamic, midbrain-thalamic, midbrain-striatal, and midbrain-hippocampal connectivity. Strong negative weights are observed between striatal-cortical, cerebellar-cortical, cortical-hippocampal, and midbrain-midbrain, and striatal-thalamic connectivity. For females, strong and moderately positive weights are observed between cortical-hippocampal, cortical-striatal, striatal-thalamic, cerebellar-hippocampal, and cerebellar-midbrain couplings. Clear patterns of moderately strong negative weights are observed in hippocampal-midbrain, cortical-cortical, cortical-cerebellar, cortical-hippocampal, cortical-cortical, thalamic-hippocampal, striatal-hippocampal, striatal-cortical, and striatal-thalamic couplings.

DISCUSSION

The motivation for this study was predicated on previous work that showed the potential of FNC as a biomarker for moderate PAE in adult rats. In the present study, our goal was to explore the translational utility of binary classification of FNC with the aim of guiding future human subjects research. We found that a QSVM kernel was significantly effective for PAE detection in females. QSVM-kernel-based classification resulted in a correct accuracy rate of 62.5% for all animals, 58.3% for males, and 79.2% for females. Characterization of QSVM weights implicate an overarching theme of

several hippocampal and cortical networks in contributing to the formation of correct classification decisions by the QSVM. Our results imply that binary classification using QSVM and female FNC data may hold translational value for the development of novel and non-invasive techniques for the identification of PAE.

Surprisingly, statistically significant classification accuracies were only observed for females using QSVM. In our previous investigation, we found males, relative to females, displayed more alterations in FNC as a result of moderate PAE (Rodriguez et al., 2016a) and thus higher classification accuracies in females were unexpected. A possible explanation for our findings may be due to differences in the processing of independent component time-courses used to assess FNC. In the present investigation, time-courses were pre-processed by detrending, regressed for motion using an approach that included temporal derivatives, and filtered to account for in-scanner movement and to reduce the potential signal contributions stemming from respiratory processes. Relatedly, modifications to time-course pre-processing may have resulted in a greater number of FNC features that met the feature selection threshold and facilitated classification in females. An alternative explanation is that the QSVM is capturing complex non-linear relationships that are beyond the scope of the conventional explanatory modeling methods (Breiman, 2001). In the present work, non-linear data features resulted in improved classification of PAE in females.

In the present study, maternal blood alcohol levels during prenatal development reached a moderate 60.8 mg/dL (Davies et al., 2019). In rat studies of PAE, maternal alcohol serum levels can range from 30mg/dL (Cullen, Burne, Lavidis, & Moritz, 2014) in light exposure to 300 mg/dL (Mooney & Varlinskaya, 2011) in heavier exposure models.

Furthermore, the alcohol-exposed offspring in the present investigation did not produce any detectable differences in brain volume measured by structural MRI nor blood perfusion in the frontal cortex measured by arterial spin labeling when assessed in adulthood and compared to their corresponding control groups (Rodriguez et al., 2016a). Taken together, these points suggest that the classification accuracy for females is achieved despite moderate levels of PAE, the absence of gross brain morphological abnormalities, and alterations in vascular function.

The results presented here, must also be considered within the context of a number of limitations. First, the successful SVM method in our results was non-linear which decreased our ability of establishing one-to-one relationships between specific brain abnormalities and PAE, thereby reducing interpretability of the computational model developed for classification. However, this disadvantage is compensated by the enhanced ability of detecting PAE in females. Second, the FNC data utilized was of the static form which ignores temporal variations in connectivity across the scanning period. Examination of dynamic connectivity, which can account for these variations, may lead to disparate findings as evidenced in human-subjects research with dynamic FNC approaches showing better classification performance (Hutchison et al., 2013; Vergara, Mayer, Kiehl, & Calhoun, 2018). Third, the neuroimaging data utilized to subsequently measure FNC was gathered from rodents under light isoflurane anesthesia. This approach was chosen to minimize the influence of motion during image acquisition. An alternative approach could have employed the use of animal restraining devices to overcome anesthetic-related influences on brain function (King et al., 2005). Such devices used with rats and voles have revealed modest contributions of stress in normal

and awake animals after an acclimation procedure (Liang, King, & Zhang, 2011, 2012; Reed, Pira, & Febo, 2013; Yee et al., 2016). However, changes in the sensitivity of stress-related circuitry including the hippocampus and the hypothalamic-pituitary-adrenal (HPA) axis following PAE are well documented (Hellemans et al., 2008; Lam et al., 2018; Raineki, Ellis, & Weinberg, 2018), and carry the potential to introduce a different set of confounds in an awake scanning procedure with PAE rodents. Fourth, animals in this investigation reached adulthood by the time image acquisition was conducted. Thus, additional research will need to examine machine learning detection in earlier developmental periods to enhance any potential utility of this approach. Fifth, our results are based off of a total sample size of 48, and a within-sex sample size of 24 (12 PAE; 12 SAC). Consequently, the machine learning procedures employed in this report stand to benefit greatly from validation with increased sample sizes to better leverage the advantages of machine learning classifiers and may partially explain the gap in classification accuracies observed between males and females. Finally, and most importantly, we recognize the binary classification approach used in this investigation was conducted on rodent data, and any clinical applications will need be developed with human subjects.

The classification techniques used in this study have not been utilized with FNC data assessed from resting state fMRI within the context of PAE. In contrast, psychometric, structural MRI, eye tracking, and facial features have been used with binary classification and other machine learning techniques to detect PAE in human subjects. Using psychometric data alone, artificial neural networks attained an accuracy rate of 75% (Duarte, 2020). Zhang and colleagues utilized eye tracking, psychometric,

and combined eye tracking, psychometric, and diffusion tensor imaging data from children and adolescents with PAE to achieve 72%, 67%, and 78% accuracy rates respectively (Zhang et al., 2019). Using structural MRI data from children and adolescents, one study achieved a 77% classification accuracy rate (Little & Beaulieu, 2020; Zhang et al., 2019). In a study relying on a 3d facial feature scanning system, Fang and colleagues achieved an overall 80% accuracy in two ethnic samples of children with FAS (Fang et al., 2008). Thus, the QSVM method employed in the present investigation achieved a classification accuracy comparable to those previously found in the literature and suggest that this approach is feasible and may hold translational utility if applied in research with humans.

FASD continues to pose as a significant public health concern with far reaching economic, and societal consequences. The application of SVM-based classification algorithms to FNC data may serve as a potential tool that can be developed into novel and non-invasive diagnostic aids for FASD. If successful, such an approach may lead to earlier diagnoses resulting in timelier referrals to treatment and support services that may lead to improved outcomes for individuals with FASD and their caregivers.

Author Contribution Statement: Carlos Rodriguez: Conceptualization, Data curation, Software, Formal Analysis, Investigation, Visualization, Writing – Original Draft. Victor Vergara: Conceptualization, Methodology Software, Formal Analysis, Investigation, Visualization, Writing – Review & Editing, Supervision. Vince Calhoun: Conceptualization, Software, Supervision, Funding acquisition. Writing – Review & Editing. Suzy Davies: Methodology, Investigation, Resources, Writing – Review & Editing. Daniel Savage: Conceptualization, Methodology, Resources, Funding acquisition, Supervision, Writing – Review & Editing. Derek Hamilton: Conceptualization, Resources, Funding acquisition, Software, Supervision, Writing – Review & Editing.

Conflict of Interest Statement: The authors of this manuscript declare no financial nor commercial relationship that could potentially serve as conflict of interests related to this research.

Support: NIH grants P30 GM103400, P50 AA022534, and R01 AA019462

Acknowledgements: The authors would like to thank Drs. Kevin Uribe and Shawn Bates for their assistance in friendly review of this manuscript.

REFERENCES

Allen, EA, Erhardt, EB, Damaraju, E, Gruner, W, Segall, JM, Silva, RF, . . . Calhoun, VD. A baseline for the multivariate comparison of resting-state networks. Front Syst Neurosci 2011; 5:2. doi:10.3389/fnsys.2011.00002

Arbabshirani, MR, & Calhoun, VD. Functional network connectivity during rest and task: comparison of healthy controls and schizophrenic patients. Conf Proc IEEE Eng Med Biol Soc 2011; 2011:4418-4421. doi:10.1109/IEMBS.2011.6091096

Bastanlar, Y, & Ozuysal, M. Introduction to machine learning. Methods Mol Biol 2014; 1107:105-128. doi:10.1007/978-1-62703-748-8_7

Bell, AJ, & Sejnowski, TJ. An Information Maximization Approach to Blind Separation and Blind Deconvolution. Neural Computation 1995; 7(6):1129-1159. doi:Doi 10.1162/Neco.1995.7.6.1129

Bertrand, J, Floyd, LL, Weber, MK, Fetal Alcohol Syndrome Prevention Team, DoBD, Developmental Disabilities, NCoBD, Developmental Disabilities, CfDC, & Prevention. Guidelines for identifying and referring persons with fetal alcohol syndrome. MMWR Recomm Rep 2005; 54(RR-11):1-14. Retrieved from http://www.ncbi.nlm.nih.gov/pubmed/16251866

Breiman, L. Statistical modeling: The two cultures. Statistical Science 2001; 16(3):199-215. doi:DOI 10.1214/ss/1009213726

Buckner, RL, Krienen, FM, & Yeo, BT. Opportunities and limitations of intrinsic functional connectivity MRI. Nat Neurosci 2013; 16(7):832-837. doi:10.1038/nn.3423

Bzdok, D, Altman, N, & Krzywinski, M. Statistics versus machine learning. Nat Methods 2018; 15(4):233-234. doi:10.1038/nmeth.4642

Calhoun, VD, Adali, T, Pearlson, GD, & Pekar, JJ. A method for making group inferences from functional MRI data using independent component analysis. Hum Brain Mapp 2001; 14(3):140-151.

Choi, RY, Coyner, AS, Kalpathy-Cramer, J, Chiang, MF, & Campbell, JP. Introduction to Machine Learning, Neural Networks, and Deep Learning. Translational Vision Science & Technology 2020; 9(2). doi:ARTN 14

10.1167/tvst.9.2.14

Connor, PD, Sampson, PD, Bookstein, FL, Barr, HM, & Streissguth, AP. Direct and indirect effects of prenatal alcohol damage on executive function. Dev Neuropsychol 2000; 18(3):331-354. doi:10.1207/S1532694204Connor

Cullen, CL, Burne, TH, Lavidis, NA, & Moritz, KM. Low dose prenatal alcohol exposure does not impair spatial learning and memory in two tests in adult and aged rats. PLoS One 2014; 9(6):e101482. doi:10.1371/journal.pone.0101482

Davies, S, Ballesteros-Merino, C, Allen, NA, Porch, MW, Pruitt, ME, Christensen, KH, . . . Savage, DD. Impact of moderate prenatal alcohol exposure on histaminergic neurons, histidine decarboxylase levels and histamine H2 receptors in adult rat offspring. Alcohol 2019; 76:47-57. doi:10.1016/j.alcohol.2018.07.007

Duarte, VdJ. (2020, 16-20 Nov. 2020). *Artificial Neural Network techniques to distinguish children with Fetal Alcohol Spectrum Disorder from psychometric data.* Paper presented at the 2020 39th International Conference of the Chilean Computer Science Society (SCCC).

Fang, S, McLaughlin, J, Fang, J, Huang, J, Autti-Rämö, I, Fagerlund, Å, . . . Disorders, CIoFAS. Automated diagnosis of fetal alcohol syndrome using 3D facial image analysis. Orthodontics & Craniofacial Research 2008; 11(3):162-171. doi:https://doi.org/10.1111/j.1601-6343.2008.00425.x

Gil-Mohapel, J, Boehme, F, Kainer, L, & Christie, BR. Hippocampal cell loss and neurogenesis after fetal alcohol exposure: insights from different rodent models. Brain Res Rev 2010; 64(2):283-303. doi:10.1016/j.brainresrev.2010.04.011

Green, CR, Mihic, AM, Nikkel, SM, Stade, BC, Rasmussen, C, Munoz, DP, & Reynolds, JN. Executive function deficits in children with fetal alcohol spectrum disorders (FASD) measured using the Cambridge Neuropsychological Tests Automated Battery (CANTAB). J Child Psychol Psychiatry 2009; 50(6):688-697. doi:10.1111/j.1469-7610.2008.01990.x

Hamilton, DA, Magcalas, CM, Barto, D, Bird, CW, Rodriguez, CI, Fink, BC, . . . Savage, DD. Moderate Prenatal Alcohol Exposure and Quantification of Social Behavior in Adult Rats. Jove-Journal of Visualized Experiments 2014; (94). doi:ARTN e52407

10.3791/52407

Hastie, TT, R.; Friedman, J. (2009). *The Elements of Statistical Learning : Data Mining, Inference, and Prediction*(2nd ed. ed.).

Hellemans, KG, Verma, P, Yoon, E, Yu, W, & Weinberg, J. Prenatal alcohol exposure increases vulnerability to stress and anxiety-like disorders in adulthood. Ann N Y Acad Sci 2008; 1144:154-175. doi:10.1196/annals.1418.016

Hutchison, RM, Womelsdorf, T, Allen, EA, Bandettini, PA, Calhoun, VD, Corbetta, M, . . . Chang, C. Dynamic functional connectivity: promise, issues, and interpretations. Neuroimage 2013; 80:360-378. doi:10.1016/j.neuroimage.2013.05.079

Jones, KL, & Smith, DW. Recognition of the fetal alcohol syndrome in early infancy. Lancet 1973; 302(7836):999-1001.

Jones, KL, & Smith, DW. The fetal alcohol syndrome. Teratology 1975; 12(1):1-10. doi:10.1002/tera.1420120102

King, JA, Garelick, TS, Brevard, ME, Chen, W, Messenger, TL, Duong, TQ, & Ferris, CF. Procedure for minimizing stress for fMRI studies in conscious rats. J Neurosci Methods 2005; 148(2):154-160. doi:10.1016/j.jneumeth.2005.04.011

Lam, VYY, Raineki, C, Ellis, L, Yu, W, & Weinberg, J. Interactive effects of prenatal alcohol exposure and chronic stress in adulthood on anxiety-like behavior and central stress-related receptor mRNA expression: Sex- and time-dependent effects. Psychoneuroendocrinology 2018; 97:8-19. doi:10.1016/j.psyneuen.2018.06.018

Lemoine, P, Harousseau, H, Borteyru, JP, & Menuet, JC. Children of Alcoholic Parents - Anomalies in 127 Cases. Archives Francaises De Pediatrie 1968; 25(7):830-+. Retrieved from <Go to ISI>://WOS:A1968B838800015

Liang, Z, King, J, & Zhang, N. Uncovering intrinsic connectional architecture of functional networks in awake rat brain. J Neurosci 2011; 31(10):3776-3783. doi:10.1523/JNEUROSCI.4557-10.2011

Liang, Z, King, J, & Zhang, N. Anticorrelated resting-state functional connectivity in awake rat brain. Neuroimage 2012; 59(2):1190-1199. doi:10.1016/j.neuroimage.2011.08.009

Little, G, & Beaulieu, C. Multivariate models of brain volume for identification of children and adolescents with fetal alcohol spectrum disorder. Hum Brain Mapp 2020; 41(5):1181-1194. doi:10.1002/hbm.24867

Logothetis, NK, Pauls, J, Augath, M, Trinath, T, & Oeltermann, A. Neurophysiological investigation of the basis of the fMRI signal. Nature 2001; 412(6843):150-157. doi:10.1038/35084005

Loock, C, Conry, J, Cook, JL, Chudley, AE, & Rosales, T. Identifying fetal alcohol spectrum disorder in primary care. CMAJ 2005; 172(5):628-630. doi:10.1503/cmaj.050135

Manning, MA, & Eugene Hoyme, H. Fetal alcohol spectrum disorders: a practical clinical approach to diagnosis. Neurosci Biobehav Rev 2007; 31(2):230-238. doi:10.1016/j.neubiorev.2006.06.016

Mattson, SN, Bernes, GA, & Doyle, LR. Fetal Alcohol Spectrum Disorders: A Review of the Neurobehavioral Deficits Associated With Prenatal Alcohol Exposure. Alcohol Clin Exp Res 2019; 43(6):1046-1062. doi:10.1111/acer.14040

Mattson, SN, & Riley, EP. A review of the neurobehavioral deficits in children with fetal alcohol syndrome or prenatal exposure to alcohol. Alcohol Clin Exp Res 1998; 22(2):279-294.

May, PA, Baete, A, Russo, J, Elliott, AJ, Blankenship, J, Kalberg, WO, . . . Hoyme, HE. Prevalence and characteristics of fetal alcohol spectrum disorders. Pediatrics 2014; 134(5):855-866. doi:10.1542/peds.2013-3319

May, PA, Chambers, CD, Kalberg, WO, Zellner, J, Feldman, H, Buckley, D, . . . Hoyme, HE. Prevalence of Fetal Alcohol Spectrum Disorders in 4 US Communities. Jama-Journal of the American Medical Association 2018; 319(5):474-482. doi:10.1001/jama.2017.21896

May, PA, & Gossage, JP. Estimating the prevalence of fetal alcohol syndrome. A summary. Alcohol Res Health 2001; 25(3):159-167.

Mooney, SM, & Varlinskaya, EI. Acute prenatal exposure to ethanol and social behavior: effects of age, sex, and timing of exposure. Behavioural Brain Research 2011; 216(1):358-364. doi:10.1016/j.bbr.2010.08.014

Patten, AR, Fontaine, CJ, & Christie, BR. A comparison of the different animal models of fetal alcohol spectrum disorders and their use in studying complex behaviors. Front Pediatr 2014; 2:93. doi:10.3389/fped.2014.00093

Paxinos, G, & Watson, C. (2004). *The Rat Brain in Stereotaxic Coordinates - The New Coronal Set* (5th ed.): Academic Press.

Popova, S, Stade, B, Bekmuradov, D, Lange, S, & Rehm, J. What do we know about the economic impact of fetal alcohol spectrum disorder? A systematic literature review. Alcohol Alcohol 2011; 46(4):490-497. doi:10.1093/alcalc/agr029

Raichle, ME, & Mintun, MA. Brain work and brain imaging. Annu Rev Neurosci 2006; 29:449-476. doi:10.1146/annurev.neuro.29.051605.112819

570 Raineki, C, Ellis, L, & Weinberg, J. Impact of adolescent stress on the expression of
571 stress-related receptors in the hippocampus of animals exposed to alcohol
572 prenatally. Hippocampus 2018; 28(3):201-216. doi:10.1002/hipo.22823
573 Reed, MD, Pira, AS, & Febo, M. Behavioral effects of acclimatization to restraint
574 protocol used for awake animal imaging. J Neurosci Methods 2013; 217(1-2):63-
575 66. doi:10.1016/j.jneumeth.2013.03.023
576 Rodriguez, CI, Davies, S, Calhoun, V, Savage, DD, & Hamilton, DA. Moderate Prenatal
577 Alcohol Exposure Alters Functional Connectivity in the Adult Rat Brain. Alcohol
578 Clin Exp Res 2016a; 40(10):2134-2146. doi:10.1111/acer.13175
579 Rodriguez, CI, Magcalas, CM, Barto, D, Fink, BC, Rice, JP, Bird, CW, . . . Hamilton, DA.
580 Effects of sex and housing on social, spatial, and motor behavior in adult rats
581 exposed to moderate levels of alcohol during prenatal development. Behavioural
582 Brain Research 2016b; 313:233-243. doi:10.1016/j.bbr.2016.07.018
583 Savage, DD, Becher, M, de la Torre, AJ, & Sutherland, RJ. Dose-dependent effects of
584 prenatal ethanol exposure on synaptic plasticity and learning in mature offspring.
585 Alcohol Clin Exp Res 2002; 26(11):1752-1758.
586 doi:10.1097/01.ALC.0000038265.52107.20
587 Schweinhardt, P, Fransson, P, Olson, L, Spenger, C, & Andersson, JL. A template for
588 spatial normalisation of MR images of the rat brain. J Neurosci Methods 2003;
589 129(2):105-113.
590 Servais, L, Hourez, R, Bearzatto, B, Gall, D, Schiffmann, SN, & Cheron, G. Purkinje cell
591 dysfunction and alteration of long-term synaptic plasticity in fetal alcohol

syndrome. Proc Natl Acad Sci U S A 2007; 104(23):9858-9863. doi:10.1073/pnas.0607037104

Snyder, AZ, & Raichle, ME. A brief history of the resting state: the Washington University perspective. Neuroimage 2012; 62(2):902-910. doi:10.1016/j.neuroimage.2012.01.044

Streissguth, AP, Barr, HM, Sampson, PD, Parrishjohnson, JC, Kirchner, GL, & Martin, DC. Attention, Distraction and Reaction-Time at Age 7 Years and Prenatal Alcohol Exposure. Neurobehavioral Toxicology and Teratology 1986; 8(6):717-725. Retrieved from <Go to ISI>://WOS:A1986F500000016

Streissguth, AP, Bookstein, FL, Barr, HM, Sampson, PD, O'Malley, K, & Young, JK. Risk factors for adverse life outcomes in fetal alcohol syndrome and fetal alcohol effects. Journal of Developmental and Behavioral Pediatrics 2004; 25(4):228-238. doi:Doi 10.1097/00004703-200408000-00002

Vergara, VM, Mayer, AR, Kiehl, KA, & Calhoun, VD. Dynamic functional network connectivity discriminates mild traumatic brain injury through machine learning. Neuroimage Clin 2018; 19:30-37. doi:10.1016/j.nicl.2018.03.017

Williams, JF, Smith, VC, & Committee On Substance, A. Fetal Alcohol Spectrum Disorders. Pediatrics 2015. doi:10.1542/peds.2015-3113

Yarkoni, T, & Westfall, J. Choosing Prediction Over Explanation in Psychology: Lessons From Machine Learning. Perspect Psychol Sci 2017; 12(6):1100-1122. doi:10.1177/1745691617693393

Yee, JR, Kenkel, WM, Kulkarni, P, Moore, K, Perkeybile, AM, Toddes, S, . . . Ferris, CF. BOLD fMRI in awake prairie voles: A platform for translational social and

affective neuroscience. Neuroimage 2016; 138:221-232.
doi:10.1016/j.neuroimage.2016.05.046

Zhang, C, Paolozza, A, Tseng, PH, Reynolds, JN, Munoz, DP, & Itti, L. Detection of Children/Youth With Fetal Alcohol Spectrum Disorder Through Eye Movement, Psychometric, and Neuroimaging Data. Front Neurol 2019; 10:80.
doi:10.3389/fneur.2019.00080

622

623 **Table 1.** Anatomical locations of extracted components. Components are arranged according to the Paxinos and Watson
624 rat atlas (Paxinos & Watson, 2004) coordinates from anterior to posterior within regional grouping. Cortex (COR),
625 hippocampus (HIP), midbrain (MID), striatum (STR), and cerebellum (CER). Reprinted with permission (Rodriguez et al.,
626 2016a) with modified labels to reflect the acronyms used in this study.

Component Number & Label		Coordinates in (AP, ML, DV)			Abbreviation & Area	.
39	COR1	1.5	0.1	-2.7	Cg2	cingulate cortex, area 2
15	COR2	-0.1	3.5	-2.9	S1FL	primary somatosensory cortex, forelimb region
24	COR3	-3.3	-1.9	-1.5	LPtA	lateral parietal association cortex
32	COR4	-8.7	-2.1	-1.7	V2MM /V1M	secondary visual cortex, medo medial/primary visual cortex
3	HIP1	-5.1	2.1	-3.3	DS	dorsal subiculum
34	HIP2	-5.1	-5.3	-6.9	MoDG	molecular layer of the dentate gyrus
30	HIP3	-5.9	4.9	-6.3	Or	Oriens layer of the hippocampus
23	HIP4	-6.1	-3.1	-4.1	MoDG	molecular layer of the dentate gyrus
17	HIP5	-6.3	-5.5	-5.5	Lmol	lacunosum moleculare layer of the hippocampus
1	MID1	-3.5	-1.9	-7.7	ZID/ZI V	zona incerta dorsal/zona incerta ventral
18	MID2	-6.3	2.5	-4.7	InG	intermediate gray layer of the superior colliculus
6	MID3	-8.3	1.7	-2.7	ECIC	external cortex of the inferior colliculus

14	STR1	2.1	2.3	-4.3	Cpu	Caudate Putamen
25	STR2	-0.7	1.3	-4.9	LSI	lateral septal nucleus, intermediate part
40	THL1	-1.7	-1.9	-5.9	VA/VL	region where VA and VL overlap (ventral anterior thalamic nucleus/ventrolateral thalamic nucleus)
16	THL2	-3.1	1.7	-6.1	Po	posterior thalamic nuclear group
10	CER1	-11.7	-1.5	-5.1	MedDL	medial cerebellar nucleus, dorsolateral protuberance

627

628

629

630 **Table 2. Classification accuracy rates of different SVM kernels.** Support vector machine (SVM), radial basis function

631 (RBF), multilayer perceptron (MLP). * significant at Bonferroni corrected (α = 0.05/5) threshold.

SVM Kernel	All Samples %	Males %	Females %
Linear	54.0	50.0	66.7
Quadratic	62.5	58.3	79.2*
Cubic	60.4	41.7	66.7
RBF	50.0	58.3	70.8
MLP	54.2	54.2	66.7

632

Figure 1.

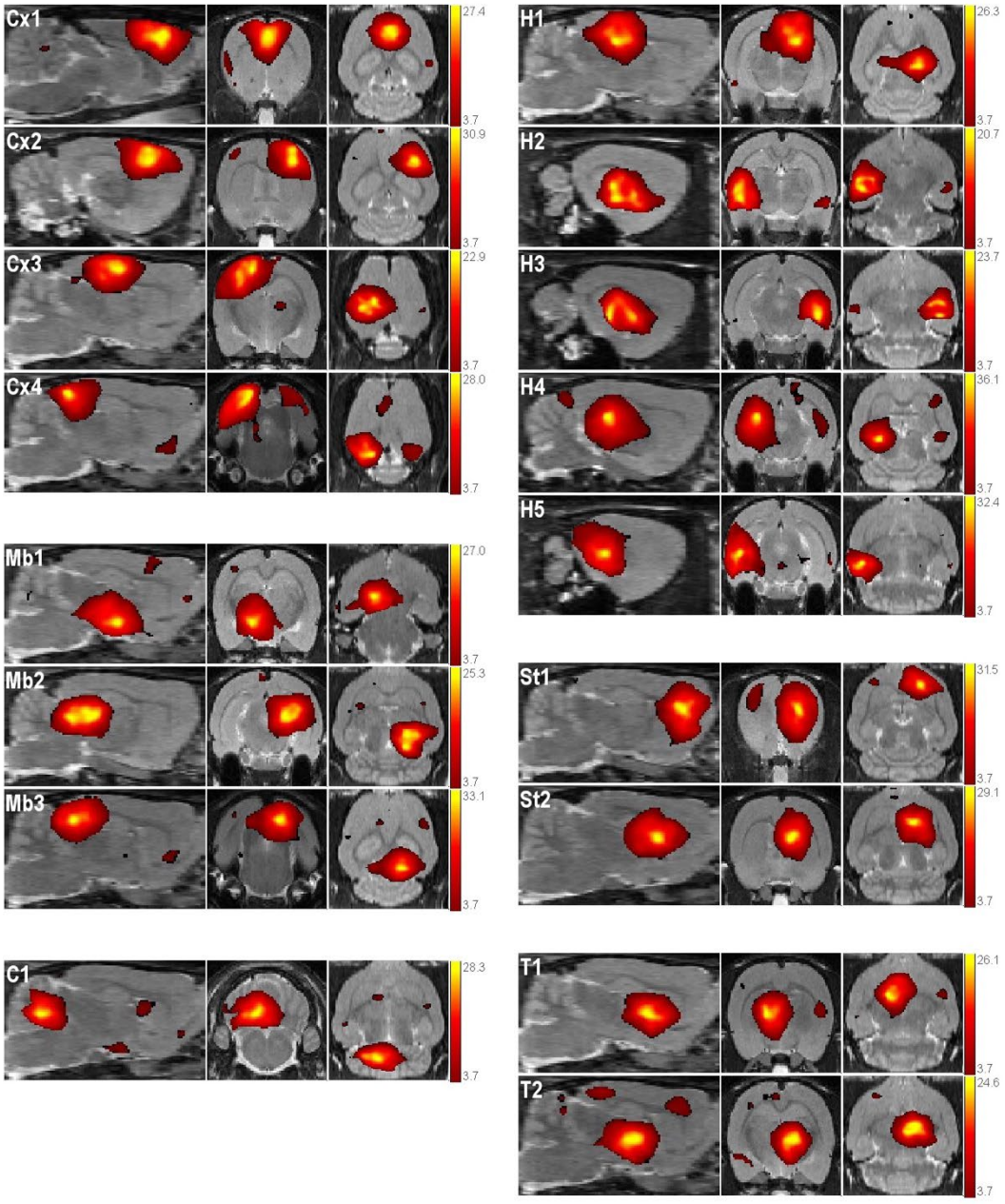

Figure 1. Retained independent components. Independent components in sagittal, coronal, and axial views. Independent component time courses were used to assess FNC. The anatomic location of the peak component t-value determined grouping into cortical (Cx), midbrain (Mb),

hippocampal (H), striatal (St), cerebellar (C) and thalamic (T) networks. Reprinted with permission (Rodriguez, Davies, et al., 2016).

Figure 2.

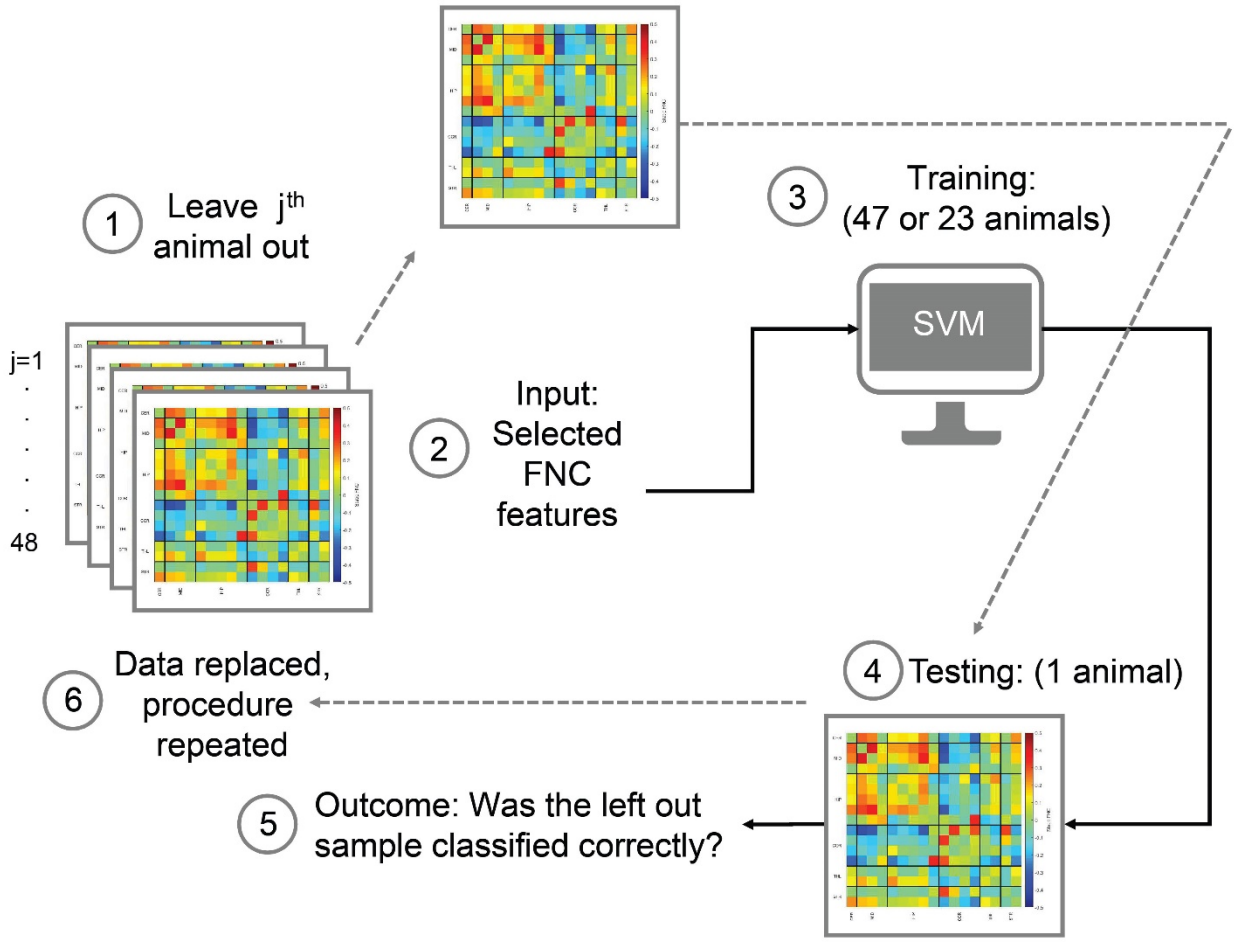

Figure 2. Schematic for the machine learning workflow. FNC matrices represent the 136 pairwise correlations between independent component time-courses (blue=negative correlations, red=positive correlations) for each subject. The number of iterations was dependent on the number of animals in the sample. For each iteration, (1) the connectivity matrix from the j^{th} subject was left out, (2) the remaining matrices (47 in the case for all animals,

24 for males or females) underwent feature selection via absolute t-value threshold which served as input for (3) training one of five SVM binary-classification kernels. The computational model developed during training is then (4) tested on the left out FNC data and decisions were (5) verified as correct or incorrect. Finally, the j^{th} subject data is replaced (6) and the procedure repeated leaving the next animal out. The procedure was repeated until all classification decisions were gathered and verified. Correct classification decisions out of 48 (all animals) or 24 (males or females) comprise accuracy rates. Dotted lines represent the workflow of the leave-one-out cross validation procedure, while the solid line represents the machine learning workflow of training and testing.

Figure 3.

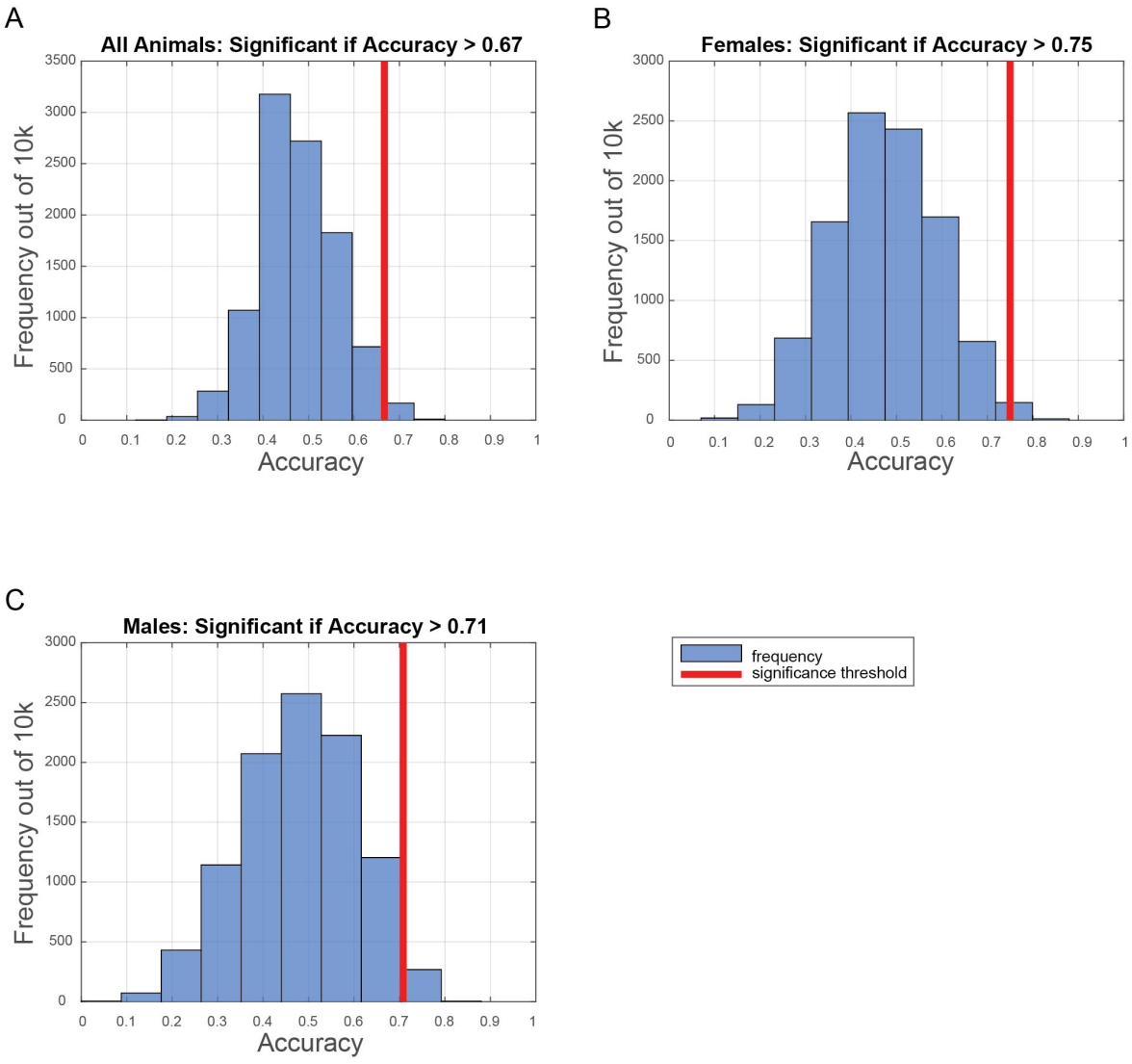

Figure 3. Null-model classification accuracy histograms. Histograms illustrate the SVM classification accuracies after prenatal condition labels were randomized and subjected to 10,000 iterations of LOOCV. The resulting distribution of accuracy rates under the null model provided the basis for calculating the probability of obtaining an accuracy rate equal to or greater than the observed SVM classification accuracy rates for A) all animals, B) females, and

C) males (i.e. p-values). Significance is set at a Bonferroni corrected level $\alpha = 0.05/5$ ($\alpha = 0.01$) to correct for the five different kernels tested.

Figure 4.

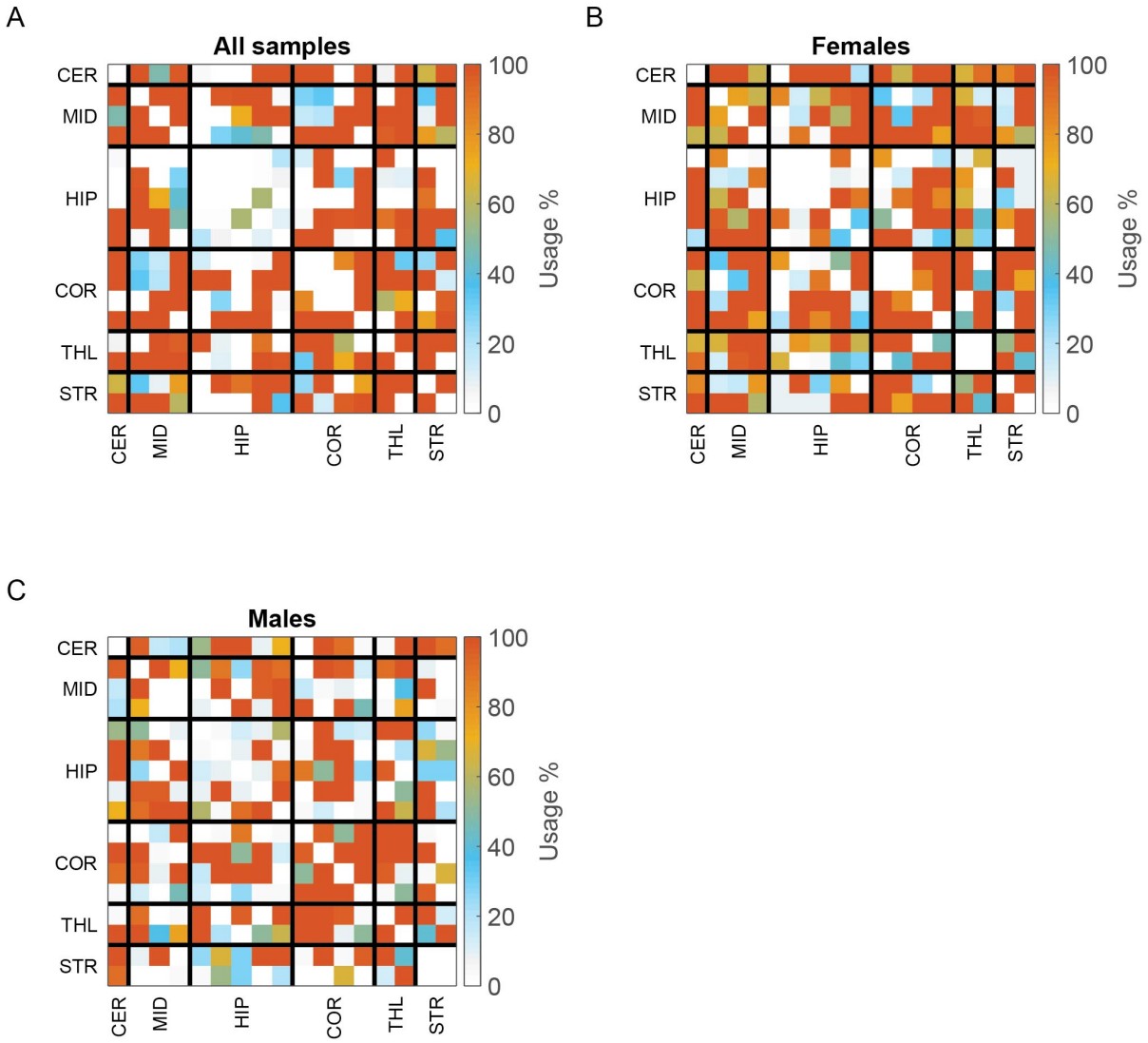

Figure 4. Usage percentages. Cells display usage percentage of FNC values as features in all iterations of LOOCV for (A) all animals (48 iterations), (B) females (24 iterations), and (C) males (24 iterations). Cells within a network are ordered numerically, for example, the use percentage of the first hippocampal component is displayed along the first row of the HIP grouping that is

predominantly characterized by a row of white cells in panel A. Component labels correspond to striatal (STR), thalamic (THL), cortical (COR), hippocampal (HIP), midbrain (MID), and cerebellar (CER) networks. LOOCV, leave-one-out-cross-validation.

Figure 5.

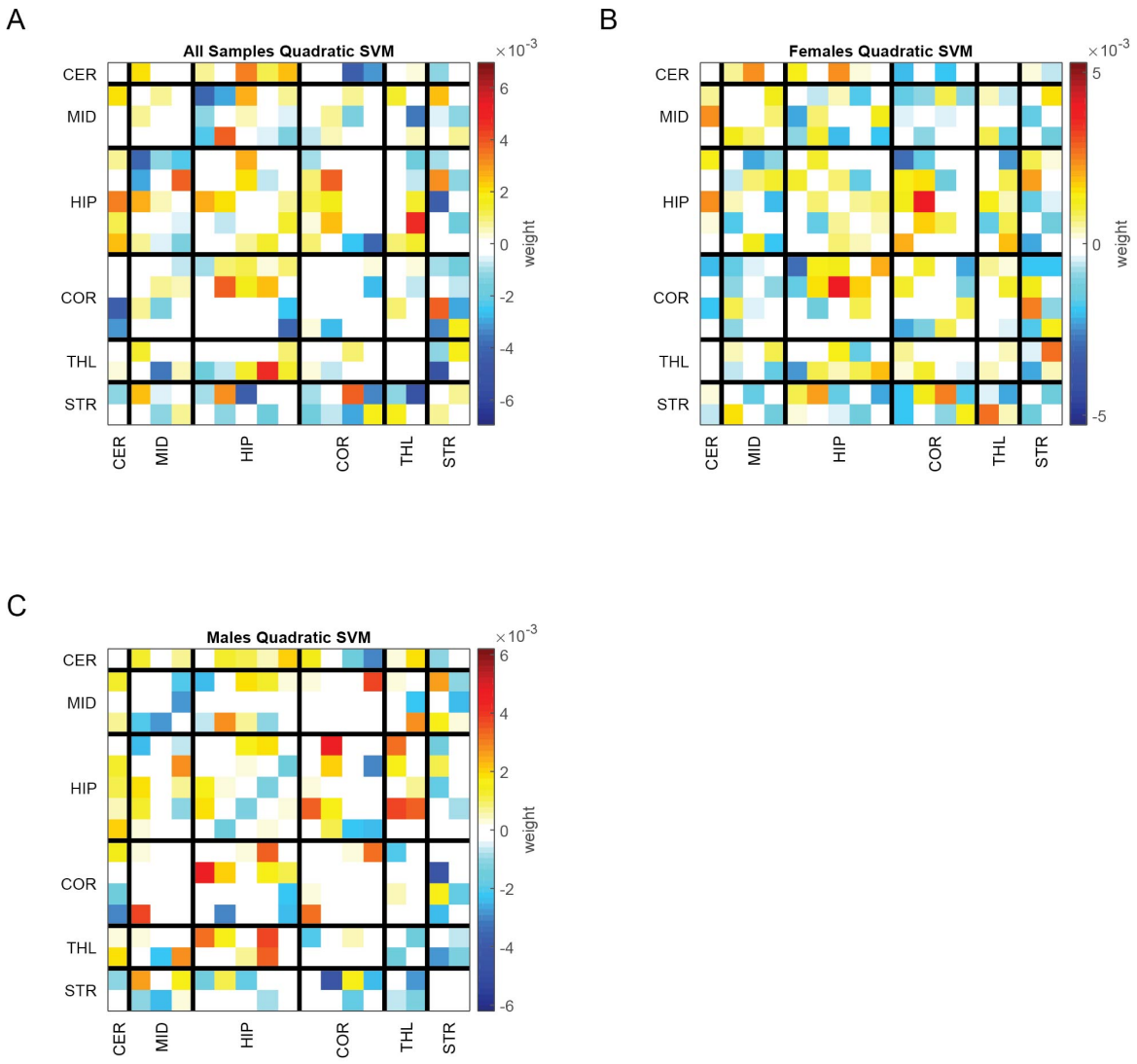

Figure 5. Mean QSVM weights. Cells display mean weights for pairwise correlation values used in quadratic SVM classification decisions for (A) all animals, (B) females, and (C) males. Component labels correspond to striatal (STR), thalamic (THL), cortical (COR), hippocampal (HIP), midbrain (MID), and cerebellar (CER) networks. SVM, support vector machine.

Supplementary Figure 1.

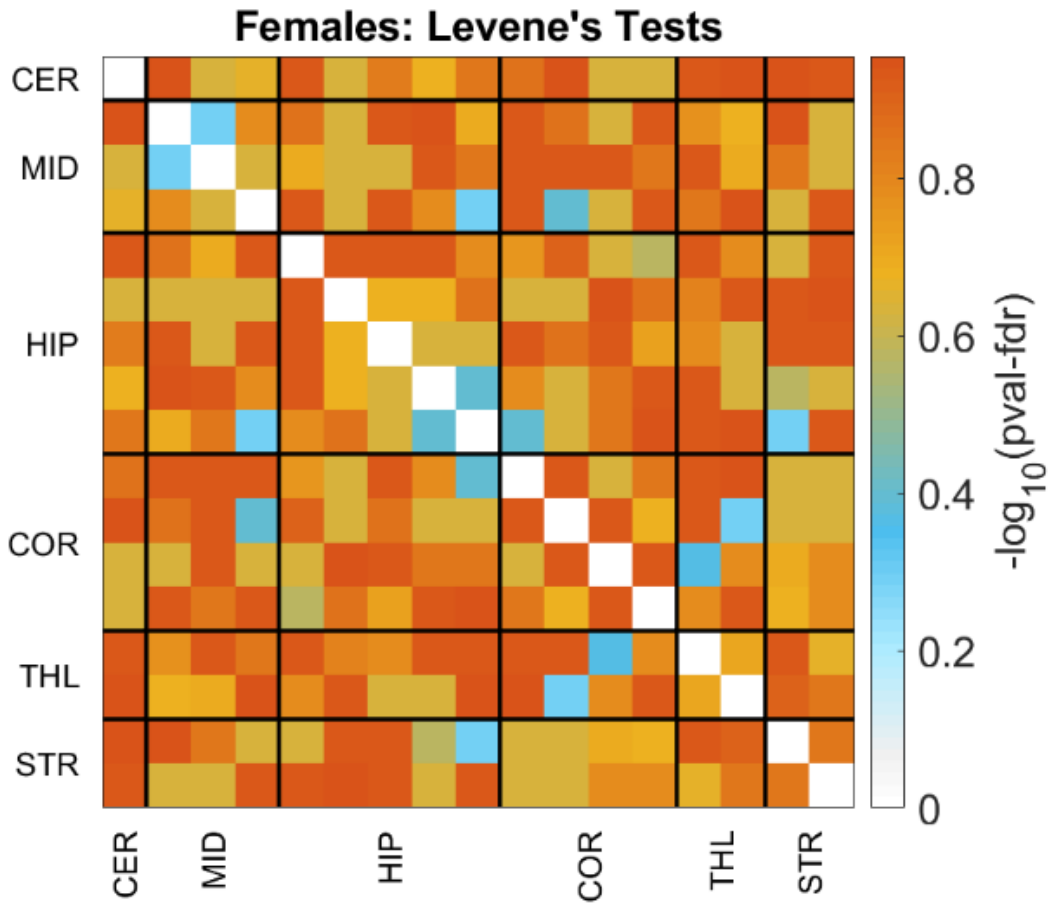

Supplementary Figure 1. Levene's tests for homogeneity of variance. False discovery rate (FDR) corrected p-values resulting from a series of Levene's tests of homogeneity of variance between female PAE and SAC FNC values. Component labels correspond to striatal (STR), thalamic (THL), cortical (COR), hippocampal (HIP), midbrain (MID), and cerebellar (CER) networks.